RESEARCH ARTICLE

BATTERIES

A rechargeable zinc-air battery based on zinc peroxide chemistry

Wei Sun[1], Fei Wang[2]*, Bao Zhang[3], Mengyi Zhang[1], Verena Küpers[1], Xiao Ji[4], Claudia Theile[1], Peter Bieker[1], Kang Xu[5]*, Chunsheng Wang[4,6]*, Martin Winter[1,7]*

Rechargeable alkaline zinc-air batteries promise high energy density and safety but suffer from the sluggish 4 electron (e^-)/oxygen (O_2) chemistry that requires participation of water and from the electrochemical irreversibility originating from parasitic reactions caused by caustic electrolytes and atmospheric carbon dioxide. Here, we report a zinc-O_2/zinc peroxide (ZnO_2) chemistry that proceeds through a $2e^-/O_2$ process in nonalkaline aqueous electrolytes, which enables highly reversible redox reactions in zinc-air batteries. This ZnO_2 chemistry was made possible by a water-poor and zinc ion (Zn^{2+})–rich inner Helmholtz layer on the air cathode caused by the hydrophobic trifluoromethanesulfonate anions. The nonalkaline zinc-air battery thus constructed not only tolerates stable operations in ambient air but also exhibits substantially better reversibility than its alkaline counterpart.

Metal-air batteries provide tantalizing solutions to the next-generation energy storage systems (*1*–*3*), among which zinc-air batteries (ZABs) are of interest for their potential low cost, high safety, environmental friendliness, and high energy density (*4*). Most previous efforts focus on a Zn anode and a porous carbonaceous air cathode in alkaline aqueous electrolytes (*5*). As a nonrechargeable chemistry, primary alkaline ZABs have been known since the 19th century, with successful commercial products in medical and telecommunication applications, such as miniature hearing aids and wireless messaging devices (*6*, *7*). However, the key challenge for a reversible ZAB comes from the strongly alkaline electrolyte, which is chemically unstable toward the active cathode material (ambient air) and, to a large extent, causes electrochemical irreversibility at the Zn metal anode (*8*). Zn metal in an alkaline environment suffers from formation of dendrites with high surface area, well known from Li metal anodes (*9*, *10*), nonuniform electrodeposition and electrodissolution, and persistent corrosion that consumes electrolyte (*11*). To counter this, a considerable excess of Zn has to be used, leading to substantial underutilization of its theoretical capacity (*12*). On the cathode side, the reaction between alkaline electrolytes and CO_2 in air produces insoluble carbonate salts, which irreversibly consumes electrolyte and also physically clogs and chemically deactivates the porous air cathode (*13*). Hence, neat O_2 atmosphere instead of ambient air is usually required (*14*, *15*), inducing complicated cell designs and a further reduction in energy density. Because the redox reaction of O_2 occurs through a sluggish 4 electron (e^-) O–O bond cleavage and formation pathway in conventional alkaline electrolytes, bifunctional catalysts have to be used on the cathode (*16*).

Efforts to improve the reversibility of ZABs have focused on developing bifunctional catalysts for the air cathode (*17*) or prolonging the Zn anode life span by electrode architecture design or electrolyte additives (*11*, *18*). Recent efforts have demonstrated that near-neutral aqueous electrolytes could suppress the formation of Zn dendrite and carbonates (*19*, *20*). Highly reversible Zn electrodeposition and electrodissolution were also achieved in certain superconcentrated electrolytes (*12*). However, the core challenge presented by a sluggish $4e^-$ pathway oxygen reduction reaction (ORR) chemistry at the cathode remained unexplored.

In most aqueous metal-air batteries using alkaline electrolytes and metals such as Zn, magnesium, iron, and aluminum, H_2O always participates in the ORR reaction through a $4e^-$ pathway producing OH^- (*21*), which constitutes the root of the poor reversibility. By contrast, an alternative $2e^-$ ORR reaction has been known as the dominating pathway in certain nonaqueous metal-air batteries, such as Li-O_2 batteries with Li_2O_2 as a product (*22*), in which the $4e^-$ ORR is suppressed. Superconcentrated electrolytes such as "water-in-salt" electrolytes provide a transition region between aqueous and nonaqueous realms. There have been reports showing that an aprotic ORR reaction could occur in water-in-salt electrolytes (*23*), in which the H_2O was excluded from the primary solvation structures of the cations (*24*). By comparing the hydrophobicity of three anions of Zn salts (fig. S1), we selected the hydrophobic trifluoromethanesulfonate (OTf^-) anion with a large size as a constituent of the electrolyte solute. Because hydrophobic OTf^- anion will absorb on the cathode surface because of the electrostatic force, a localized H_2O-poor environment will be created in the inner Helmholtz layer (IHL) (*25*), enabling the aprotic $2e^-$ ORR reaction in a dilute aqueous electrolyte.

Zn-air cells in nonalkaline electrolytes

Ambient air was used as the cathode active agent in all Zn-air cell configurations (fig. S2). Nonalkaline electrolyte of 1 mol kg^{-1} $Zn(OTf)_2$ presents a well-defined discharge plateau at ~1.0 V with an areal capacity of 52 mA·hour cm^{-2}, corresponding to a specific capacity of 684 mA·hour g^{-1} (based on Zn anode) and a Zn utilization ratio (ZUR) of 83.1% (Fig. 1A). By contrast, only an 8.1% ZUR was achieved in alkaline electrolyte consisting of 6 mol kg^{-1} KOH. The photographs of pristine and cycled Zn anodes in different electrolytes confirm the high ZUR in the $Zn(OTf)_2$ electrolyte, in which most of the Zn foil dissolved. At higher rates of 0.3 and 1 mA cm^{-2}, 70.8 and 52.9% ZUR could be achieved (fig. S3A). Replacing the Zn foil with Zn powder further increased the ZUR to 93.7% (fig. S3B).

After resting in the KOH electrolyte for 24 hours, the open circuit voltage (OCV) of the Zn-air cell starts fluctuating, followed by a lower discharge plateau and capacity fading (Fig. 1B), indicating the poor storage and discharge performance of the Zn-air cell with KOH electrolyte. By contrast, a rather stable OCV persists in the $Zn(OTf)_2$ electrolyte for 480 hours, followed by a flat discharge plateau at ~1.0 V, indicating stable discharge. The $Zn(OTf)_2$ electrolyte also enabled a more stable performance in an on-off discharge procedure that emulated a practical duty cycle (fig. S4, A and B). Persistent corrosion of the Zn anode in KOH electrolyte (*26*) can be confirmed by x-ray diffraction (XRD) patterns and photographs (fig. S4C), whereas Zn anodes in $Zn(OTf)_2$ electrolyte basically maintain the pristine surface. Zn reversibility was further investigated using Zn‖Zn symmetrical cells (fig. S5), in which the voltage profiles of repeated electrodeposition and electrodissolution of Zn metal anode in the $Zn(OTf)_2$ electrolyte remained stable after more than 150 hours (75 cycles),

[1]MEET Battery Research Center, Institute of Physical Chemistry, University of Münster, Münster, Germany. [2]Department of Materials Science, Fudan University, Shanghai, China. [3]School of Optical and Electronic Information, Huazhong University of Science and Technology, Wuhan, Hubei, China. [4]Department of Chemical and Biomolecular Engineering, University of Maryland, College Park, MD, USA. [5]Energy Storage Branch, Biomaterials and Energy Division, Sensor and Electro Devices Directorate, U.S. Army Research Laboratory, Adelphi, MD, USA. [6]Department of Chemistry and Biochemistry, University of Maryland, College Park, MD, USA. [7]Helmholtz Institute Münster, IEK-12, Forschungszentrum Jülich GmbH, Münster, Germany.
*Corresponding author. Email: martin.winter@uni-muenster.de (M.W.); cswang@umd.edu (C.W.); conrad.k.xu.civ@mail.mil (K.X.); feiw@fudan.edu.cn (F.W.)

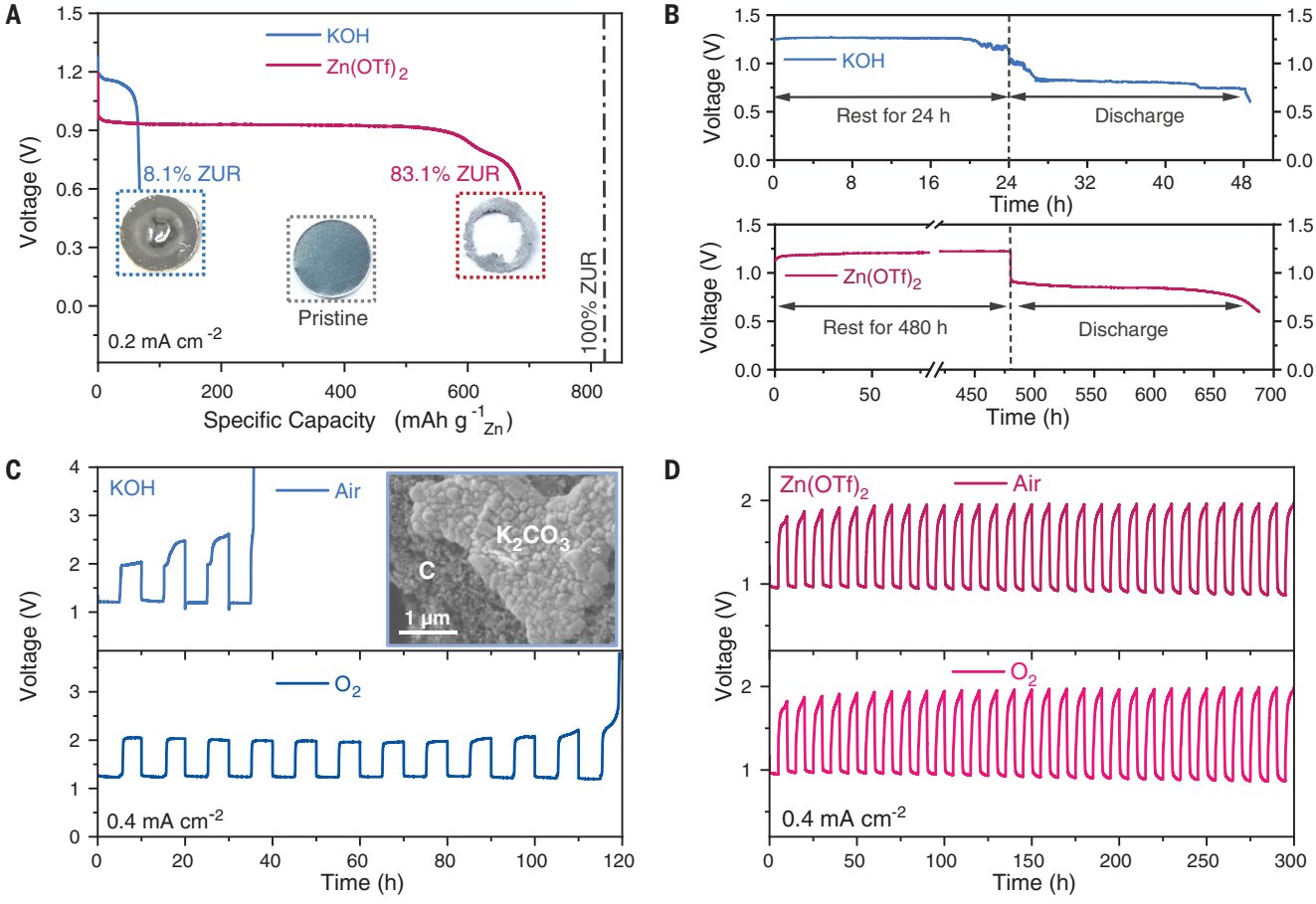

Fig. 1. Electrochemical performance of Zn-air cells in a $Zn(OTf)_2$ electrolyte (1 mol kg^{-1}) and in a conventional KOH electrolyte (6 mol kg^{-1}). (**A**) Galvanostatic discharge profiles of Zn-air cells in KOH (blue) and $Zn(OTf)_2$ (red) electrolytes at 0.2 mA cm^{-2} (cutoff voltage: 0.6 V). The corresponding ZURs were indexed for comparison. Insets are photographs of the pristine Zn anode (middle), the Zn anode after discharge in KOH (left), and $Zn(OTf)_2$ (right) electrolytes. mAh, mA·hour. (**B**) Storage performance of Zn-air cells using KOH (24-hour rest before discharge) and $Zn(OTf)_2$ (480-hour rest before discharge) electrolytes. (**C** and **D**) Galvanostatic discharge and charge profiles of Zn-air cells in (C) KOH and (D) $Zn(OTf)_2$ electrolytes in a capacity fixed mode (fixed capacity: 2 mA·hour cm^{-2}) at 0.4 mA cm^{-2} under air and O_2 atmosphere, respectively. Inset is an SEM image of the air cathode after two cycles in KOH electrolyte under air atmosphere.

whereas a sudden increase in polarization occurred within only six cycles in the KOH electrolyte, indicating Zn dendrite formation. Using XRD and scanning electron microscopy (SEM), after only two cycles, a ZnO passivation layer was detected on the Zn anode recovered from the KOH electrolyte, whereas no new reflections appeared on Zn recovered from $Zn(OTf)_2$ electrolyte (fig. S6A). After cycling, a considerable morphology change was observed on Zn recovered from the KOH electrolyte (fig. S6, B and C), whereas the Zn deposition morphology remained relatively uniform in the $Zn(OTf)_2$ electrolyte (fig. S6D).

On the cathode side, K_2CO_3 was observed after only two cycles in the KOH electrolyte, apparently generated by the reaction between KOH and the CO_2 in air (fig. S7A). K_2CO_3 precipitation clogged the porous structure of the air cathode and insulated the electron pathways (inset of Fig. 1C and fig. S7, B and C), contributing to severe loss of cathode activity and capacity fading. The separator also turned brown after cycling in the KOH electrolyte, indicating carbon corrosion (*27*) (fig. S7E). In comparison, no apparent change could be found at both the air cathode and separator after cycling in the $Zn(OTf)_2$ electrolyte (fig. S7). As a result, the Zn-air cell in the KOH electrolyte lasted for only three cycles. Replacing air with neat O_2 extended the life of such a cell to more than 12 cycles (Fig. 1C). When resting in neat CO_2, the OCV of the Zn-air cell started fluctuating immediately (fig. S8), showing the sensitivity of alkaline electrolyte toward CO_2. In the $Zn(OTf)_2$ electrolyte, however, the cells delivered similar performance in air and neat O_2 (Fig. 1D). To further confirm the reproducibility, two identical cells were constructed and then cycled under either air or neat O_2, and the identical behavior verified the air tolerance of $Zn(OTf)_2$ electrolytes (fig. S9).

Besides $Zn(OTf)_2$ electrolytes, a $ZnSO_4$-based electrolyte was considered as another non-alkaline alternative to the KOH electrolyte with better electrochemical reversibility (*28*–*30*). Using a pH-monitoring cell (fig. S2B), we tracked the electrolyte pH value for both $Zn(OTf)_2$ and $ZnSO_4$ during operation of the Zn-air cells. The $Zn(OTf)_2$ electrolyte maintained a stable pH in both the discharge (ORR) and the charge [oxygen evolution reaction (OER)] processes, but the pH of the $ZnSO_4$ electrolyte increased steadily during discharge (ORR) and decreased during charge (OER), apparently as a result of OH^- generation during ORR and consumption during OER (Fig. 2A). In extended cycling, the $Zn(OTf)_2$ electrolyte maintained a stable pH value (fig. S10).

To identify the discharge products, air cathodes were disassembled from the discharged Zn-air cells. Additional XRD patterns were indexed to ZnO_2 on the cathode recovered from the $Zn(OTf)_2$ electrolytes (Fig. 2B). The absence of any other diffraction reflections except ZnO_2 indicated that no other well-crystallized

products were formed, which is further confirmed by energy-dispersive x-ray mapping, Raman, and O1s x-ray photoelectron spectroscopy, respectively (figs. S11 and S12). As revealed by SEM (inset of Fig. 2B and fig. S11B), the formed ZnO_2 had a fiber structure within the scale of a few hundred nanometers. Upon recharge, ZnO_2 completely disappeared from XRD, SEM, and Raman spectra (Fig. 2B and figs. S11C and S12B), demonstrating its electrochemical reversibility. Combined with ex situ XRD at different states of discharge and charge (fig. S12, C and D), fully reversible ZnO_2 formation and decomposition chemistry can be established during cycling in the $Zn(OTf)_2$ electrolyte. The chemical stability of ZnO_2 in $Zn(OTf)_2$ electrolyte as well as in neat water was also evidenced by XRD that showed no major changes during 30 days of storage (fig. S13).

In $ZnSO_4$ electrolyte, zinc sulfate hydroxide [$Zn_4(OH)_6SO_4{\cdot}0.5H_2O$ (ZHS)] was identified as a discharge product (Fig. 2C and fig. S14, A to D). The formed ZHS had a typical large flake-like structure at the scale of tens of micrometers, consistent with (*31*, *32*). Upon charging, part of the insulating ZHS flakes remained, because of its poor reversibility in the $ZnSO_4$ electrolyte (fig. S14E).

The difference in electrochemical behavior caused by these two electrolytes could be attributed to the respective reaction mechanisms. The number of e^- (Z) transferred to O_2 during ORR or OER was determined by measuring the O_2 consumption or evolution and the corresponding charge transfer based on the ideal gas law and Faraday's law (*33*). The pressure decrease of a Zn-O_2 cell in $Zn(OTf)_2$ was about two times that in the $ZnSO_4$ electrolyte, corresponding to a 1.97e^- transfer per O_2 molecule (e^-/O_2) in $Zn(OTf)_2$ and a 3.79e^-/O_2 in $ZnSO_4$ (Fig. 2D and fig. S15). The pressure of the Zn-O_2 cell using $Zn(OTf)_2$ electrolyte is

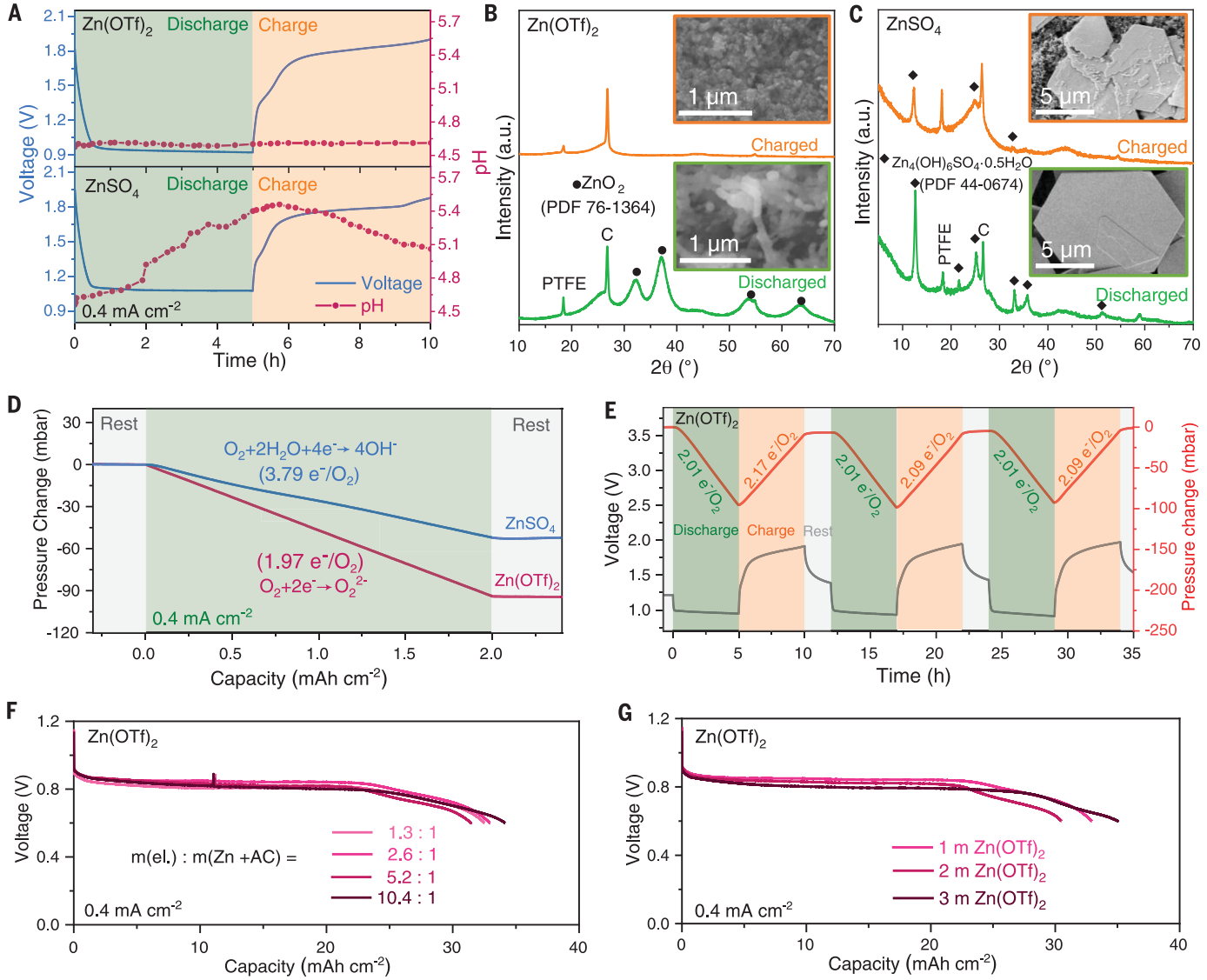

Fig. 2. Elucidating electrochemical reaction mechanisms of Zn-air cells in $Zn(OTf)_2$ (1 mol kg^{-1}) and $ZnSO_4$ (1 mol kg^{-1}) electrolytes. (**A**) Typical second-cycle galvanostatic discharge and charge profiles of Zn-air cells using $Zn(OTf)_2$ and $ZnSO_4$ electrolytes at 0.4 mA cm^{-2} and the corresponding recorded electrolyte pH values. (**B** and **C**) XRD patterns and SEM images of air cathodes obtained after discharge and recharge in (B) $Zn(OTf)_2$ and (C) $ZnSO_4$ electrolytes, respectively. a.u., arbitrary units; C, carbon; PDF, powder diffraction file; PTFE, polytetrafluoroethylene. (**D**) Pressure change in the gas reservoir of Zn-O_2 cells using $Zn(OTf)_2$ and $ZnSO_4$ electrolytes during a discharge process under neat O_2 atmosphere. (**E**) Pressure change of Zn-O_2 cells using $Zn(OTf)_2$ electrolyte during galvanostatic discharge and charge at 0.4 mA cm^{-2}. (**F** and **G**) Typical galvanostatic discharge profiles of Zn-air cells using $Zn(OTf)_2$ electrolyte (F) with varying mass ratios of electrolyte to electrodes [Zn anode and air cathode, m(el.):m(Zn + AC)] and (G) with varying salt concentrations at 0.4 mA cm^{-2}. AC, air cathode; el., electrolyte; m, mol kg^{-1}.

reversible, as shown in Fig. 2E, where the pressure increased back to the starting value when a discharge and charge cycle finished, confirming the reversible O_2 consumption and evolution during the cycling. The Z values in multiple discharging processes are all close to $2e^-/O_2$, corresponding to the formation of ZnO_2. However, Z values in these charging processes are slightly higher than 2, which might originate from minor H_2O decomposition with a $4e^-/O_2$ pathway.

Combining the aforementioned findings about the discharge product and pH value during the discharge and charge process, the overall reaction of the ZAB chemistry in $Zn(OTf)_2$ can be expressed as reversible ZnO_2 formation and decomposition (Eq. 1)

$$Zn + O_2 \leftrightarrow ZnO_2 \quad (1)$$

whereas the cell reaction in $ZnSO_4$ electrolytes is reversible ZHS formation and decomposition (Eq. 2)

$$2Zn + O_2 + \frac{2}{3}ZnSO_4 + \frac{7}{3}H_2O \leftrightarrow \frac{2}{3}Zn_4(OH)_6SO_4{\cdot}0.5H_2O\downarrow \quad (2)$$

The ORR reaction in the $ZnSO_4$ electrolyte generates OH^-, similar to that in conventional alkaline (KOH) electrolytes (*34*, *35*). $ZnSO_4$ will subsequently react with OH^-, creating a complex hydrate ZHS (*31*). In other words, ZHS in this case is limited by the availability of $ZnSO_4$ or H_2O from the electrolyte, in contrast with the cathode ORR reaction in the $Zn(OTf)_2$ electrolyte, in which no electrolyte should be consumed. The reversible ZnO_2 formation and decomposition mechanism resembles that involving Li_2O_2 formation at the cathode in nonaqueous Li-O_2 batteries (*36*, *37*). The two different mechanisms thus lead to substantially different dependences of the cell capacity on the amount of electrolyte. The capacity delivered in $ZnSO_4$ electrolytes is restricted by the electrolyte amount (fig. S16), whose steady consumption will also induce a drop in ion conductivity; hence, excessive electrolyte is needed to maintain a discharge and charge reaction over cycling, at the expense of practical energy density. When using $Zn(OTf)_2$ electrolytes with different electrolyte/electrode mass ratios, essentially identical discharge performance was obtained (Fig. 2F). Similar discharge curves were also demonstrated in the concentration range of $Zn(OTf)_2$ from 1 to 3 mol kg^{-1} (Fig. 2G and fig. S17). Therefore, the $2e^-/O_2$ reaction mechanism enabled by $Zn(OTf)_2$ electrolyte not only offers a reversible ZAB chemistry but also makes it possible to construct high–energy density ZABs with lean electrolyte volume. An alternative zinc salt with larger fluorinated anion, zinc bis(trifluoromethanesulfonyl)imide [$Zn(TFSI)_2$], was also evaluated. Similar electrochemical performance and cell reaction products were observed with 1 mol kg^{-1} $Zn(TFSI)_2$ (fig. S18), verifying that "superconcentration" is not needed as long as a proper anion is selected.

ZnO_2 formation mechanism

Multiscale simulations were used to understand the origin for the different mechanisms observed in different Zn-ion electrolytes. Molecular dynamics simulations showed that the bulk liquid structures in 1 mol kg^{-1} $Zn(OTf)_2$ and $ZnSO_4$ electrolytes were similar, in which Zn^{2+} was coordinated with about six H_2O molecules (fig. S19, A to D). However, a major difference existed between the hydrophobicity of SO_4^{2-} and OTf^- owing to the strongly hydrophobic CF_3 group on OTf^- (fig. S19, E and F). This difference is reflected in the fact that

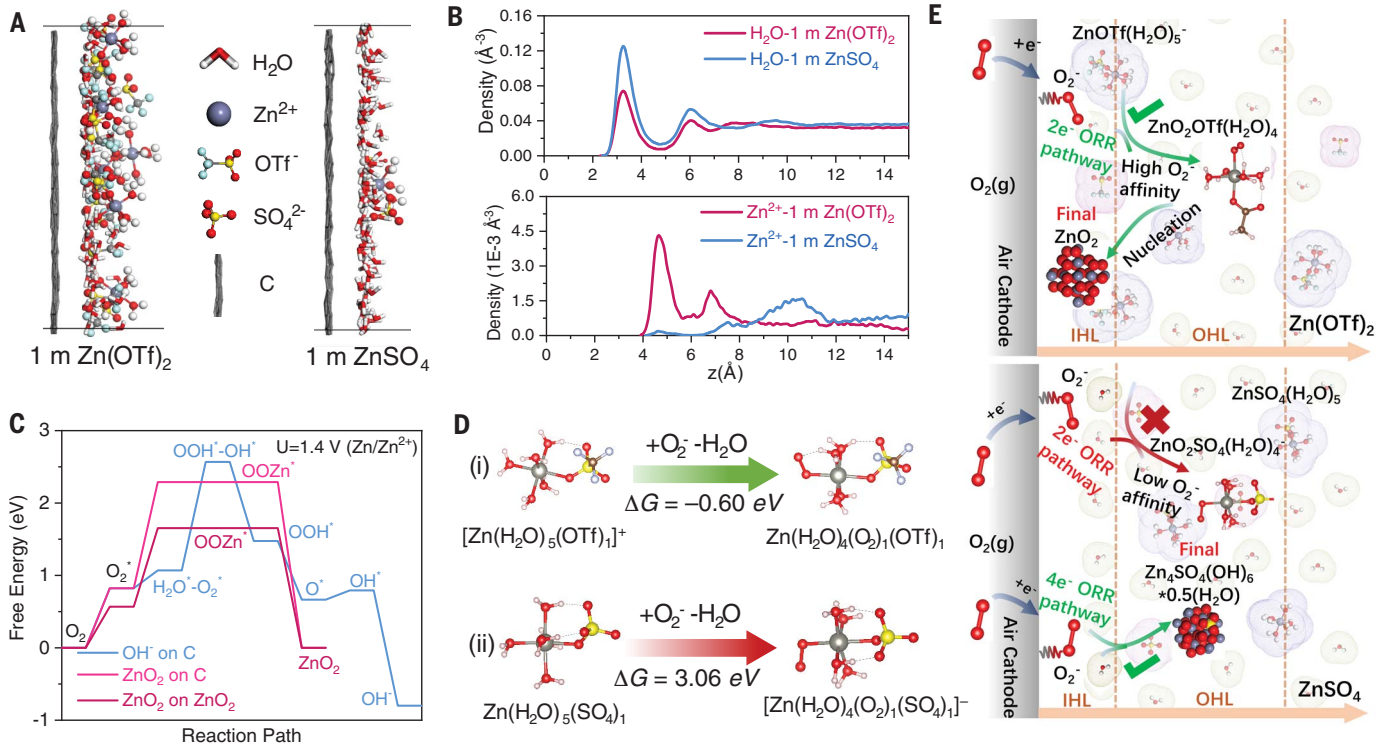

Fig. 3ORR mechanism in $Zn(OTf)_2$ and $ZnSO_4$ electrolytes. (**A**) Schematic snapshots (side view) of the interfacial structures at the air cathodes in $Zn(OTf)_2$ and $ZnSO_4$ electrolytes with positive applied potential (U = 1.4 V versus Zn/Zn^{2+}). (**B**) Corresponding interfacial cumulated density profiles of the H_2O and Zn^{2+} in the $Zn(OTf)_2$ and $ZnSO_4$ electrolytes, respectively. z, distance from the cathode surface. (**C**) Free-energy diagrams of ORR processes with a reaction path through OH^- on the C surface, through ZnO_2 formation on the C surface, and through ZnO_2 formation on ZnO_2 surface (U = 1.4 V versus Zn/Zn^{2+}). (**D**) Desolvation and superoxide-containing ion pair formation process in (i) $Zn(OTf)_2$ and (ii) $ZnSO_4$ electrolytes. (**E**) Schematic illustration of reaction processes in the IHL and outer Helmholtz layer (OHL) at the surface of the air cathode in $Zn(OTf)_2$ and $ZnSO_4$ electrolytes, respectively.

commercial $Zn(OTf)_2$ salt is normally available as anhydrous powder, whereas $ZnSO_4$ salt usually comes in the form of hydrated crystals (fig. S1). Such hydrophobicity disparity directly determined the behavior of these anions when assembling at the air cathode surface, leading to distinctly different electrochemical double-layer structures. At an applied potential of $U = 0.8$ V versus Zn/Zn^{2+} (simulated potential of zero charge), the hydrophobic OTf^- anions created an H_2O-poor environment, whereas the hydrophilic SO_4^{2-} anion led to an H_2O-rich environment at the IHL (fig. S20, A to C). Positive deviation of the applied potential toward $U = 1.4$ V versus Zn/Zn^{2+} (simulated potential of positive charge) further enriched the population of the hydrophobic OTf^- anions in the IHL of the cathode, which simultaneously decreased the H_2O presence and reduced the opportunity of H_2O-related reactions (Fig. 3A and fig. S20, D and E). By contrast, the IHL-H_2O molecular ratio experienced little change in the $ZnSO_4$ electrolyte as the potential shifted. Most of the Zn^{2+} ions were expelled from the IHL in the $ZnSO_4$ electrolyte, whereas abundant Zn^{2+} ions in the $Zn(OTf)_2$ electrolyte remained within a distance of 6 Å from the cathode. Such interfacially accumulated density profiles of Zn^{2+} and H_2O indicated that more Zn^{2+} but less H_2O molecules assembled near the air cathode in the $Zn(OTf)_2$ electrolyte than in the $ZnSO_4$ electrolyte (Fig. 3B). This relatively H_2O-poor and Zn^{2+}-rich IHL environment created by a $Zn(OTf)_2$ electrolyte reduced the opportunity of H_2O-related reactions but provided better access to Zn^{2+} for the ORR process.

Density functional theory calculations were also performed to predict possible ORR pathways. Two reaction mechanisms ($2e^-$ and $4e^-$ transfer) were compared for reactions involving both Zn^{2+} and H_2O (fig. S21). After excluding those with higher free-energy barriers, the two most probable pathways, i.e., the $2e^-$ transfer with Zn^{2+} and the $4e^-$ transfer with H_2O on the carbon surface, remained (Fig. 3C). The overpotential of the Zn^{2+}-involving $2e^-$ mechanism was slightly lower than that of the H_2O-involving $4e^-$ mechanism, mainly because of the sluggish and difficult H–OH bond cleaving process. Hence, the $4e^-$ H_2O decomposition pathway should be disfavored in $Zn(OTf)_2$ electrolytes. As ZnO_2 formation on its own surface would encounter a much lower free-energy barrier, ZnO_2 growth should follow an accelerated process once overcoming the initial nucleation stage, which is in good agreement with the SEM images after different discharge times (fig. S22).

Quantum chemistry calculations reveal that the weak affinity between Zn^{2+} cations and OTf^- anions in $Zn(OTf)_2$ electrolyte favors the formation of superoxide-containing ion pairs and advances the subsequent $2e^-$ pathway mechanism involving Zn^{2+}, whereas the higher affinity between Zn^{2+} cations and SO_4^{2-} anions inhibits Zn^{2+} desolvation and the subsequent formation process of superoxide-containing ion pairs (Fig. 3D and fig. S23). The predicted ORR processes inside the electrochemical double layer near the cathode surface in different electrolytes are summarized in Fig. 3E, where an H_2O-poor and Zn^{2+}-rich structure brought in by the hydrophobic nature of the OTf^- anions and the weak affinity between Zn^{2+} cations and OTf^- anions are the two main contributors to the preferred $2e^-$ ORR chemistry, leading to the highly reversible ZnO_2 formation, which is impossible in electrolytes using highly hydrophilic anions such as SO_4^{2-}.

Highly reversible Zn-air cells in $Zn(OTf)_2$ electrolytes

The rate performance of the Zn-air cells was examined at different current densities with a fixed capacity of 8 mA·hour cm^{-2} (Fig. 4A). Corresponding XRD patterns of air cathodes after discharging and charging confirmed reversible ZnO_2 formation and oxidation at different current densities (Fig. 4B and fig. S24). A slightly increasing polarization was observed when the current increased from 0.1 to 2.0 mA cm^{-2}. At a high current of 4.0 mA cm^{-2}, the large overpotential could

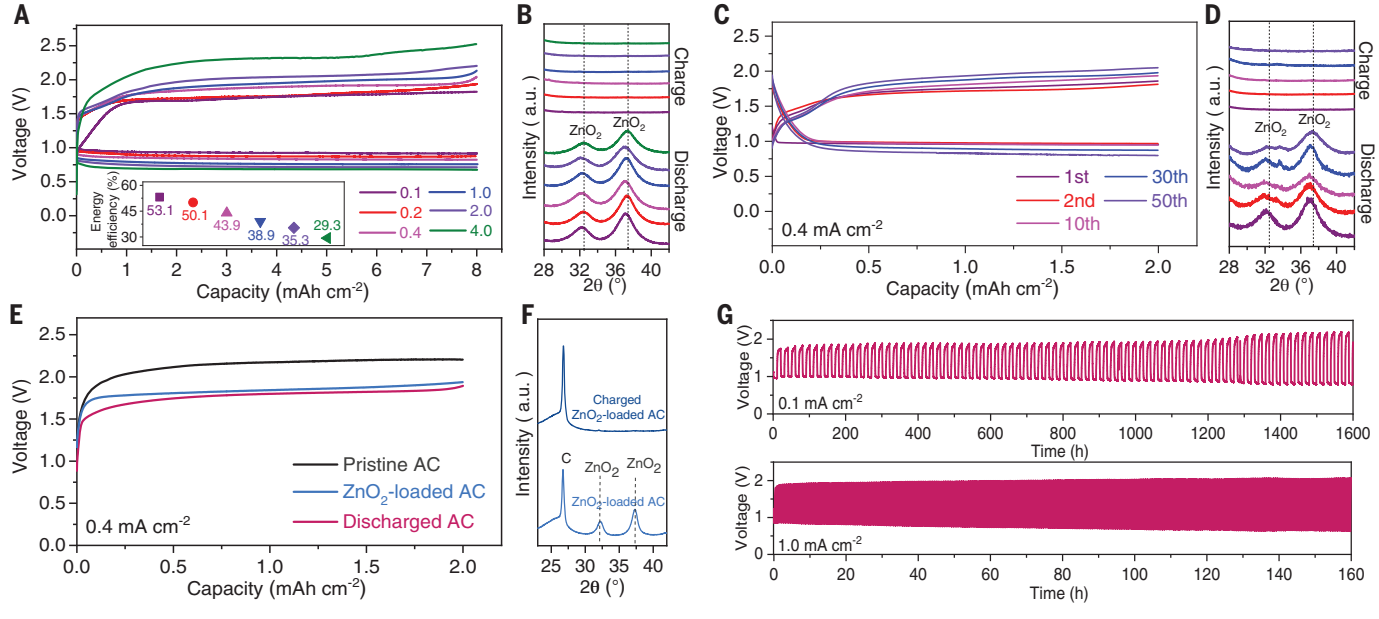

Fig. 4. Cycling stability of Zn-air cells based on ZnO_2. (**A**) Galvanostatic voltage profiles and energy efficiencies (inset) of the Zn-air cells in a capacity fixed mode (fixed capacity: 8.0 mA·hour cm^{-2}) at current densities of 0.1, 0.2, 0.4, 1.0, 2.0, and 4.0 mA cm^{-2}. (**B**) Corresponding XRD patterns of air cathodes obtained after discharge and charge at different current densities. (**C**) Galvanostatic voltage profiles of the Zn-air cell in a capacity fixed mode (fixed capacity: 2.0 mA·hour cm^{-2}) at a current density of 0.4 mA cm^{-2}. (**D**) Corresponding XRD patterns of air cathodes obtained after different cycles. (**E**) Galvanostatic charge profiles of the pristine air cathode, the ZnO_2-loaded air cathode, and the discharged air cathode. (**F**) Corresponding XRD patterns of the ZnO_2-loaded air cathodes before and after charge. (**G**) Long-term cycling performance of Zn-air cells at current densities of 0.1 and 1.0 mA cm^{-2}.

lead to oxidation of H_2O. Therefore, powerful catalysts for the $2e^-$ ORR or OER reaction are still needed for better energy efficiency. Without catalysts, the round-trip energy efficiencies (<55%, inset of Fig. 4A) of the Zn-air cell are relatively low when compared with those of Li-ion battery technology (>90%) (*38*, *39*). However, the overvoltage observed for this nonalkaline ZAB is already comparable to many alkaline ZABs and Li-O_2 batteries using catalysts (table S1). As demonstrated in the three-electrode cells, the high overvoltage of the Zn-air full cells mainly comes from the ORR and OER at the air cathode (fig. S25). One would infer that a proper bifunctional catalyst or redox mediator may further lower the overpotential at the cathode and improve the energy efficiency. Two approaches, carbon cathode modification and increased temperature, can be adopted to reduce the overpotential of air cathodes (fig. S26).

The Zn-air cell demonstrated no apparent polarization increase after 50 cycles at 0.4 mA cm^{-2} (Fig. 4C). XRD patterns during different cycles reveal that the ZnO_2 formed during discharge fully vanished after the subsequent charge process (Fig. 4D and fig. S27), further corroborating the reversibility of the O_2/ZnO_2 redox reaction. The electrochemical reversibility of ZnO_2 was further confirmed by charging chemically synthesized ZnO_2 in a similar air cell setup (Fig. 4E and fig. S28A). By loading the synthesized ZnO_2 into an air cathode (ZnO_2-loaded AC), it delivered a similar charge behavior as the electrochemically formed ZnO_2 in the air cathode (discharged AC), differing from the blank carbon cathode (pristine AC), in which only electrolyte decomposition occurred. XRD and SEM images revealed the disappearance of ZnO_2 after charging (Fig. 4F and fig. S28, B to D), indicating the high electrochemical activity of ZnO_2. The gas compositions of the Zn-air cell after charging and overcharging were analyzed using a gas chromatography–thermal conductivity detector. Most of the gas was O_2, with no CO_2 detected, again confirming the reversibility of ZnO_2 but also indicating the absence of carbon corrosion in the air cathode (fig. S29).

The Zn-air cell operated stably for 1600 hours in ambient air at a current density of 0.1 mA cm^{-2} with a 10-hour charge and discharge duration per cycle (Fig. 4G). When cycled at a 10-times-higher current density of 1.0 mA cm^{-2}, a stable cycling performance for 160 hours (320 cycles) was achieved. The performance from this nascent chemistry is encouraging, but a practical device still needs more engineering optimization. As demonstrated in a three-electrode Zn-air cell configuration (fig. S30), the sluggish OER and ORR at the air cathode limits the kinetics of the Zn-air cell in the short term, and the instability of the Zn metal anode eventually leads to cell failure. Moreover, because the ZAB in this work is designed to work in an open atmosphere, the electrolyte evaporation (water loss) becomes an inevitable issue, and a water management system might be needed to ensure a long-term practical operation (fig. S31). In nonalkaline electrolytes, the parasitic reactions of both the Zn anode and electrolytes could also present a challenge, owing to the H^+ activity being higher than that in the alkaline counterpart (e.g., 6 mol kg^{-1} KOH), and additional measures are needed to suppress the parasitic reactions as inspired by pioneering work (*12*, *40*). Nevertheless, to demonstrate the simplicity of fabrication and applicability of this ZnO_2 battery chemistry, a prototype square cell with more than 50 mA·hour energy storage was assembled and discharged at a large current of 20 mA (fig. S32), which displays a well-defined discharge plateau at ~1.0 V, similar to that of the experimental Swagelok cell.

We demonstrated a nonalkaline ZAB based on a reversible O_2/ZnO_2 chemistry. Comprehensive characterization and simulations identified the critical role of hydrophobic OTf^- anions in dictating the electrochemical double-layer structure that favors the formation of ZnO_2 and suppression of H_2O-involved reactions. Leveraging the high reversibility of both the air cathode and Zn metal anode in the $Zn(OTf)_2$ electrolyte, the Zn-air full cell demonstrated excellent cycling performance in ambient air despite a simple cell structure. Such tailoring of interfacial structures through electrolyte properties provides a solution to the electrochemical irreversibility that has been plaguing not only alkaline ZABs but also nearly all metal-air batteries for centuries, especially those with promising high theoretical energy densities using materials with abundance, but being only feasible in alkaline electrolytes as either primary or mechanically rechargeable batteries. Examples may include magnesium-air [theoretical specific energy: 6815 watt-hours (Wh) kg^{-1}], iron-air (1229 Wh kg^{-1}), or aluminum-air (8076 Wh kg^{-1}) (*38*).

REFERENCES AND NOTES

1. C. Xia, C. Y. Kwok, L. F. Nazar, *Science* **361**, 777–781 (2018).
2. G. Cong, W. Wang, N.-C. Lai, Z. Liang, Y.-C. Lu, *Nat. Mater.* **18**, 390–396 (2019).
3. B. J. Hopkins, Y. Shao-Horn, D. P. Hart, *Science* **362**, 658–661 (2018).
4. J. W. Choi, D. Aurbach, *Nat. Rev. Mater.* **1**, 16013 (2016).
5. H.-F. Wang, Q. Xu, *Matter* **1**, 565–595 (2019).
6. Y. Li, H. Dai, *Chem. Soc. Rev.* **43**, 5257–5275 (2014).
7. D. Stock, S. Dongmo, J. Janek, D. Schröder, *ACS Energy Lett.* **4**, 1287–1300 (2019).
8. A. R. Mainar *et al.*, *Int. J. Energy Res.* **40**, 1032–1049 (2016).
9. M. Winter, B. Barnett, K. Xu, *Chem. Rev.* **118**, 11433–11456 (2018).
10. G. Bieker, M. Winter, P. Bieker, *Phys. Chem. Chem. Phys.* **17**, 8670–8679 (2015).
11. D. E. Turney *et al.*, *Chem. Mater.* **29**, 4819–4832 (2017).
12. F. Wang *et al.*, *Nat. Mater.* **17**, 543–549 (2018).
13. J. Fu *et al.*, *Adv. Mater.* **29**, 1604685 (2017).
14. Y. Li *et al.*, *Nat. Commun.* **4**, 1805 (2013).
15. M. Prabu, K. Ketpang, S. Shanmugam, *Nanoscale* **6**, 3173–3181 (2014).
16. J. Fu *et al.*, *Adv. Mater.* **31**, 1805230 (2019).
17. F. Cheng, J. Chen, *Chem. Soc. Rev.* **41**, 2172–2192 (2012).
18. J. F. Parker *et al.*, *Science* **356**, 415–418 (2017).
19. F. W. Thomas Goh *et al.*, *J. Electrochem. Soc.* **161**, A2080–A2086 (2014).
20. C. Y. Chen, K. Matsumoto, K. Kubota, R. Hagiwara, Q. Xu, *Adv. Energy Mater.* **9**, 1900196 (2019).
21. Z.-L. Wang, D. Xu, J.-J. Xu, X.-B. Zhang, *Chem. Soc. Rev.* **43**, 7746–7786 (2014).
22. Z. Peng, S. A. Freunberger, Y. Chen, P. G. Bruce, *Science* **337**, 563–566 (2012).
23. Q. Dong *et al.*, *Chem* **4**, 1345–1358 (2018).
24. L. Suo *et al.*, *Science* **350**, 938–943 (2015).
25. O. Borodin, J. Self, K. A. Persson, C. Wang, K. Xu, *Joule* **4**, 69–100 (2020).
26. X. G. Zhang, *Corrosion and Electrochemistry of Zinc* (Plenum, 2013).
27. P. N. Ross, H. Sokol, *J. Electrochem. Soc.* **131**, 1742–1750 (1984).
28. D. Kundu, B. D. Adams, V. Duffort, S. H. Vajargah, L. F. Nazar, *Nat. Energy* **1**, 16119 (2016).
29. W. Sun *et al.*, *J. Am. Chem. Soc.* **139**, 9775–9778 (2017).
30. F. Wang *et al.*, *Energy Environ. Sci.* **11**, 3168–3175 (2018).
31. H. Pan *et al.*, *Nat. Energy* **1**, 16039 (2016).
32. J. Huang *et al.*, *Nat. Commun.* **9**, 2906 (2018).
33. P. Hartmann *et al.*, *Nat. Mater.* **12**, 228–232 (2013).
34. E. Yeager, *Electrochim. Acta* **29**, 1527–1537 (1984).
35. J. Suntivich *et al.*, *Nat. Chem.* **3**, 546–550 (2011).
36. P. G. Bruce, S. A. Freunberger, L. J. Hardwick, J.-M. Tarascon, *Nat. Mater.* **11**, 19–29 (2011).
37. A. C. Luntz, B. D. McCloskey, *Chem. Rev.* **114**, 11721–11750 (2014).
38. Y. Li, J. Lu, *ACS Energy Lett.* **2**, 1370–1377 (2017).
39. P. Meister *et al.*, *Chem. Mater.* **28**, 7203–7217 (2016).
40. J. Y. Luo, W. J. Cui, P. He, Y. Y. Xia, *Nat. Chem.* **2**, 760–765 (2010).

ACKNOWLEDGMENTS

We thank F. Horsthemke, F. J. Dohmann, and J. J. Jiang for technical support. **Funding:** This work at MEET was supported by the BMBF (Federal Ministry of Education and Research) within the projects "Mvbic" (03XP0249), "Melubatt" (03XP0110A), "MEET Hi-EnD III" (03XP0258A), and "MgMeAnS" (03XP0140). At the University of Maryland, it was supported by the U.S. Department of Energy (DOE) (through ARPA-E grant DEAR0000389), and at the Army Research Laboratory, it was supported as part of the Joint Center for Energy Storage Research, an Energy Innovation Hub funded by the DOE, Office of Science, Basic Energy Sciences (through IAA SN2020957). **Author contributions:** W.S. and F.W. conceived and designed this work. M.W., C.W., and K.X. served as technical leads for this work. W.S., F.W., M.W., C.W., and K.X. contributed to the implementation and writing of the manuscript. Data collection and analysis were conducted by W.S. and F.W. Multiscale simulation was conducted by B.Z. and X.J. SEM and Raman characterizations were conducted by W.S., M.Z., and C.T. Energy density calculation was conducted by V.K. and P.B. **Competing interests:** The authors have no competing interests. **Data and materials availability:** All data are available in the manuscript or in the supplementary materials.

SUPPLEMENTARY MATERIALS

science.sciencemag.org/content/371/6524/46/suppl/DC1
Materials and Methods
Figs. S1 to S32
Table S1
References (*41*–*68*)

2 April 2020; accepted 19 November 2020
10.1126/science.abb9554

A rechargeable zinc-air battery based on zinc peroxide chemistry

Wei Sun, Fei Wang, Bao Zhang, Mengyi Zhang, Verena Küpers, Xiao Ji, Claudia Theile, Peter Bieker, Kang Xu, Chunsheng Wang and Martin Winter

Science **371** (6524), 46-51.
DOI: 10.1126/science.abb9554

When two is better than four

Batteries based on the reaction of zinc and oxygen have been used for more than a century, but these have been primary (that is, nonrechargeable) cells. These batteries use an alkaline electrolyte and require a four-electron reduction of oxygen to water, which is a slow process. Sun *et al.* show that with the right choice of nonalkaline electrolyte, the battery can operate using a two-electron zinc-oxygen/zinc peroxide chemistry that is far more reversible. By making the electrolyte hydrophobic, water is excluded from the near surface of the cathode, thus preventing the four-electron reduction. These batteries also show higher energy density and better cycling stability.

Science, this issue p. 46